

A&amp;A manuscript no.

(will be inserted by hand later)

Your thesaurus codes are:

03(11.09.4; 11.01.1; 11.05.2; 09.01.1; 11.19.2)

ASTRONOMY  
AND  
ASTROPHYSICS

# Star formation and the interstellar medium in low surface brightness galaxies

## I. Oxygen abundances and abundance gradients in low surface brightness disk galaxies

W.J.G. de Blok\* and J.M. van der Hulst

Kapteyn Astronomical Institute, P.O. Box 800, 9700 AV Groningen, The Netherlands,  
 edeblok@physics.unimelb.edu.au, vd hulst@astro.rug.nl

Received: ; accepted:

**Abstract.** We present measurements of the oxygen abundances in 64 HII regions in 12 LSB galaxies. We find that oxygen abundances are low. No regions with solar abundance have been found, and most have oxygen abundances  $\sim 0.5$  to  $0.1$  solar. The oxygen abundance appears to be constant as a function of radius, supporting the picture of quiescently and sporadically evolving LSB galaxies.

**Key words:** Galaxies: ISM – Galaxies: abundances – Galaxies: evolution – ISM: abundances – Galaxies: spiral

### 1. Introduction

Low surface brightness (LSB) disk galaxies have all the characteristics of unevolved galaxies. Those discovered so far constitute a population of gas-rich, metal-poor galaxies with very low star formation rates (see the review by Bothun et al. 1997). Their surface brightnesses are a few magnitudes lower than the values commonly found for so-called normal galaxies. Most of them are rather late-type galaxies, with diffuse spiral arms.

A direct probe of the evolutionary state of these galaxies is the metal abundance in the interstellar medium (ISM). A low abundance generally indicates only limited enrichment of the ISM and therefore (in a closed system) a small amount of evolution.

Because of their low surface brightness, obtaining spectra of the stellar disks of LSB galaxies is difficult and requires large amounts of telescope time. Conclusions on metallicities must therefore be derived from spectra of HII regions. These usually are the brightest distinct objects in a LSB galaxy. Their bright emission lines make them more easily observable than the underlying continuum. The HII regions that are observed in LSB galaxies are usually giant HII regions, that are ionized by star clusters rather than by a few stars.

The first measurements of the oxygen abundances in HII regions in LSB galaxies were presented in McGaugh (1994). He found, using an empirical oxygen abundance indicator, that LSB galaxies are low metallicity galaxies with typical values for the metallicity  $Z < \frac{1}{3}Z_{\odot}$ . It shows that low metallicities can occur in galaxies that are comparable in size and mass to the bright galaxies that define the Hubble sequence. As LSB galaxies are found to be isolated (Mo et al. 1994), this suggests that surface mass density and environment are as important for the evolution of a galaxy as total mass.

In this paper we present a follow-up study of oxygen abundances in LSB galaxies. We confirm the results by McGaugh (1994) that LSB galaxies are metal-poor. We present two direct measurements of the oxygen abundance from measurements of the [O III] $\lambda 4363$  line, supplemented with a large number of empirically determined oxygen abundances. In addition, for those galaxies where sufficient data are available, we investigate the change in abundance with radius, and show that the measurements are consistent with no gradient. The steeper gradients found in HSB galaxies (Vila-Costas & Edmunds 1992 [VCE], Zaritsky et al. 1994, Henry & Howard 1995, Kennicutt & Garnett 1996) are not present. It is worth noting that the exact form and magnitude of the Milky Way oxygen gradient has now been consistently reproduced in early-type stars, HII regions and planetary nebulae, which supports that the extragalactic HII region gradients in HSB galaxies are real (Smarrt & Rolleston 1997).

The lack of abundance gradients in LSB galaxies supports the picture of stochastic and sporadic evolution, where the evolutionary rate only depends on local conditions and not on the global properties of LSB galaxies as a whole.

Section 2 describes the sample selection and observations. Section 3 presents the data, while in Sect. 4 the analysis is described. Section 5 discusses the abundances found. Section 6 discusses reddening towards the HII regions, while Sect. 7 concludes with presenting the gradients. In Sect. 8 the results are summarized.

Send offprint requests to: W.J.G. de Blok

\* Present address: School of Physics, University of Melbourne, Parkville VIC 3052, Australia

## 2. Sample selection, observations and reduction

LSB galaxies from the samples of van der Hulst et al. (1993) and de Blok et al. (1995) were examined for the presence of HII regions using  $H\alpha$  images. We selected as possible targets only those galaxies with two or more distinct HII regions. This introduces a bias in our sample, and it therefore cannot be considered complete in any sense. Nevertheless it makes it possible to study the ISM in a significant subset of the LSB galaxy population.

Optical spectra of 64 HII regions in 12 of the selected LSB galaxies were obtained from 6–10 February 1992 with the 4.3 meter William Herschel Telescope (WHT) at La Palma. The ISIS spectrograph was used. The gratings were adjusted such that the blue arm covered a wavelength range from  $\sim 3600$  Angstrom to  $\sim 5400$  Angstrom, while the red arm covered a range from  $\sim 5100$  Angstrom to  $\sim 6800$  Angstrom. An amount of overlap therefore existed, which was used to tie the spectra together. The resolution for both arms was 1.4 Angstrom per pixel in the dispersion direction.

Conditions during the observing run were variable: usually photometric but with seeing varying between  $2''$  and  $5''$ . Total exposure times per long-slit spectrum were 4000 seconds. A slit width of  $1''$  was used during the first two nights. This was later adjusted to  $1.6''$  for the last two nights.

The data were reduced and analyzed using standard long-slit reduction tasks from the IRAF package. Two independent reductions of the data resulted in a mean difference between integrated fluxes of the same HII regions of  $\sim 10\%$ . These systematic differences are not taken into account in further analyses, but should be kept in mind.

## 3. The Data

Figure 1 shows a few examples of LSB galaxy HII region spectra. The resulting data (uncorrected for foreground Galactic extinction which is in most cases less than 0.05 mag in  $B$ ) are presented in Tables 1 and 2.

Table 1 contains data on the hydrogen Balmer emission lines. Column 1 gives the name of the galaxy. Column 2 contains the HII region identification. The first number refers to the night the spectrum was taken; the second number is an arbitrary ranking number based on the position of the HII region along the slit.

Column 3 contains the  $H\beta$  flux in units of  $10^{-18}$  erg  $\text{cm}^{-2}$   $\text{s}^{-1}$ . The RMS error in the flux in the same units is given in Column 4. Columns 5, 6 and 7 contain the equivalent widths  $W_\lambda$  in Angstrom of the three brightest Balmer lines. The low continuum levels do however make the determination of equivalent widths uncertain. In general these could be determined only to an accuracy of  $\sim 5$  Angstrom at best. Any correction for absorption by the underlying stellar population ( $\sim 2$  Angstrom for normal galaxies [McCall et al. 1985]) will thus be negligible compared to the uncertainties in the widths themselves.

Column 8 contains the reddening coefficient  $c$ , as defined in e.g. Osterbrock (1989).  $c$  is related to  $E(B - V)$  by

$E(B - V) = 0.78c$ . Column 9 contains the error in  $c$ .  $c$  was determined from the ratio between the  $H\alpha$  and  $H\beta$  fluxes and by assuming that the HII regions were Case B HII regions with a temperature of 10,000 K (see Osterbrock 1989). We will show in Sect. 4.1 that this is a justified assumption. The interstellar extinction curve by Savage & Mathis (1979) was used. The calibration uncertainty of 10% mentioned above results in an uncertainty of 0.2 in the reddening coefficient. In a few cases negative reddenings were found. Modestly negative reddenings can usually be explained by assuming a higher temperature for the nebula combined with zero reddening. A few very negative reddenings could not be explained satisfactorily. These are noted with colons in Table 1. The spectra with negative reddenings generally have low  $H\alpha$  and  $H\beta$  fluxes thus introducing additional uncertainties. Negative reddenings have been set to zero in any further analysis.

The errors in the strong lines are shot noise limited, while the errors in the faint lines are dominated by the read-out noise of the CCD. An estimate of the uncertainty in the flux of the  $H\beta$  lines was made by adding in quadrature the shot noise in the line, the shot noise in the continuum and the read-out noise of the CCD, which is  $\sim 1 \cdot 10^{-17}$  erg  $\text{s}^{-1}$   $\text{cm}^{-2}$  for the red images, and  $\sim 5 \cdot 10^{-18}$  erg  $\text{s}^{-1}$   $\text{cm}^{-2}$  for the blue ones. To ascertain that these were realistic estimates of the uncertainties, we also determined the uncertainties in the  $H\beta$  flux by making two additional measurements of the line-flux, with the continuum levels systematically offset by  $+1\sigma$  and  $-1\sigma$  of the continuum. Both uncertainties agreed within a factor of two with each other, where for all but the strongest lines the shot noise value was slightly smaller than the offset-continuum value. The shot noise values are given in Column 4 of Table 1.

Table 2 contains the ratios of the fluxes of the other bright emission lines with respect to the  $H\beta$  flux. If additional faint lines were measured in the spectrum the HII region number is marked with a star. These extra line fluxes are given in the lower panel of Table 2.

In a few spectra the  $H\beta$  line was not detected. Fluxes of the lines that were detected in these spectra are given in Table 3. Also given in Table 3 is a  $1\sigma$  (of the continuum) upper limit of the  $H\beta$  flux. All flux values are expressed in units of  $10^{-18}$  erg  $\text{s}^{-1}$   $\text{cm}^{-2}$ .

## 4. Determining the oxygen abundances

The standard method to determine the oxygen abundance in a direct way is described by Osterbrock (1989) and involves determining the electron temperature of the gas in the HII region by measuring the ratio of intensities of the strong  $[\text{O III}]\lambda\lambda 4959, 5007$  lines and the faint  $[\text{O III}]\lambda 4363$  line. However, as can be seen in Table 2, this line was detected only with certainty in two of the best spectra (F563-1[2-3] and U5005[2-2]). We will determine the oxygen abundance of these two HII regions using the standard method in Sect. 4.1. For the other spectra the standard method does not suffice and in Sect. 4.2 we will use an empirical oxygen abundance indicator to estimate the oxygen abundances.

**Table 1.** Balmer line data

Galaxy	HII	$F(H\beta)$	$\sigma_{H\beta}$	$W_\lambda$ (H $\gamma$ )	$W_\lambda$ (H $\beta$ )	$W_\lambda$ (H $\alpha$ )	$c$	$\sigma_c$
F561-1	1-1	197	9		30	112	0.054	0.057
	1-2	574	14		47	107	0.141	0.029
F563-1	2-1	188	7	43	241	187	-0.397::	0.080
	2-2	139	7		43	102	-0.461::	0.069
	*2-3	1278	20	54	114	110	0.087	0.018
	2-4	92	6		19	103	0.709	0.087
	4-1	162	6		20	120	0.335	0.049
	4-2	1105	16	10	31	62	0.321	0.017
F563-V1	4-3	71	5		8	68	1.347	0.093
	3-2	151	7		21	52	-0.072	0.074
	3-3	104	7		14	26	-0.002	0.089
F563-V2	2-1	359	10	15	52	22	-0.174:	0.037
	2-2	588	14	28	74	239	0.191	0.029
	2-3	232	9	16	26	136	0.277	0.047
	4-1	409	11		14	92	0.519	0.031
	4-2	240	10		6	31	0.441	0.048
F568-3	2-1	193	8	20	54	145	0.250	0.050
F568-V1	3-1	103	7		6	39	0.503	0.086
F571-5	*3-1	476	11	25	272	351	-0.202:	0.028
	*3-2	1266	17	28	80	272	-0.038	0.016
F571-V1	3-1	86	4		37	85	0.370	0.086
U1230	1-1	196	7		16	323	0.072	0.054
	3-1	163	7		14	39	0.162	0.064
	3-2	145	7		43	20	-0.435::	0.110
U5005	3-6	139	7		52	2615	0.645	0.063
	2-1	156	7		49	117	0.129	0.067
	*2-2	1089	18	43	123	501	0.249	0.021
	2-3	88	6	93	51	67	-0.120:	0.104
	2-4	139	7		45	145	0.415	0.069
	2-5	103	6		18	59	0.120	0.079
	2-6	86	6		19	143	0.243	0.087
	2-7	46	5		15	47	0.105	0.143
	3-2	162	6		20	57	-0.542::	0.063
	3-3	184	10	22	42	87	0.194	0.065
U5999	3-5	154	7		29	122	-0.003	0.078
	4-1	610	13		12	51	0.442	0.026
	4-2	163	7		13	60	0.887	0.052
	3-1	185	8		14	850	0.324	0.057
	3-2	235	10		9	60	0.488	0.050
	3-3	233	8		17	103	0.170	0.047
	3-4	540	13		14	52	0.142	0.028
	4-1	163	8		8	114	-0.058	0.079
4-4	374	10		23	49	0.458	0.034	

#### 4.1. The standard method

We used the FIVEL program (De Robertis et al. 1987) as implemented in the IRAF package to iteratively solve for the electron temperature for the  $O^{++}$  region and the electron density. We refer to Table 4 for a listing of the relevant values. To determine the temperature the  $[O\ III] \lambda\lambda 4959, 5009 / [O\ III] \lambda 4363$  ratio was used; for the density the  $[S\ II] \lambda 6717 / [S\ II] \lambda 6731$  ratio. The values thus derived are consistent with the standard values for a low-density nebula of  $T_e = 10000\ K$  and  $n_e = 100\ cm^{-3}$ .

The temperature of the  $O^+$  region was calculated using the relationship given in Campbell et al. (1986):

$$T_e(O^+) = T_e(O^{++}) - 0.3[T_e(O^{++}) - 1.0],$$

with  $T_e$  expressed in units of  $10^4\ K$ . The FIVEL program was used to calculate the  $O^{++}/H^+$  and the  $O^+/H^+$  ratios, given the values of the electron density and the fluxes in the  $[O\ II] \lambda 3727$  line (which is blended with  $[O\ II] \lambda 3729$ ) and the  $[O\ III] \lambda 5007$  line. The total oxygen abundance is then given by  $O/H \equiv O^+/H^+ + O^{++}/H^+$ .

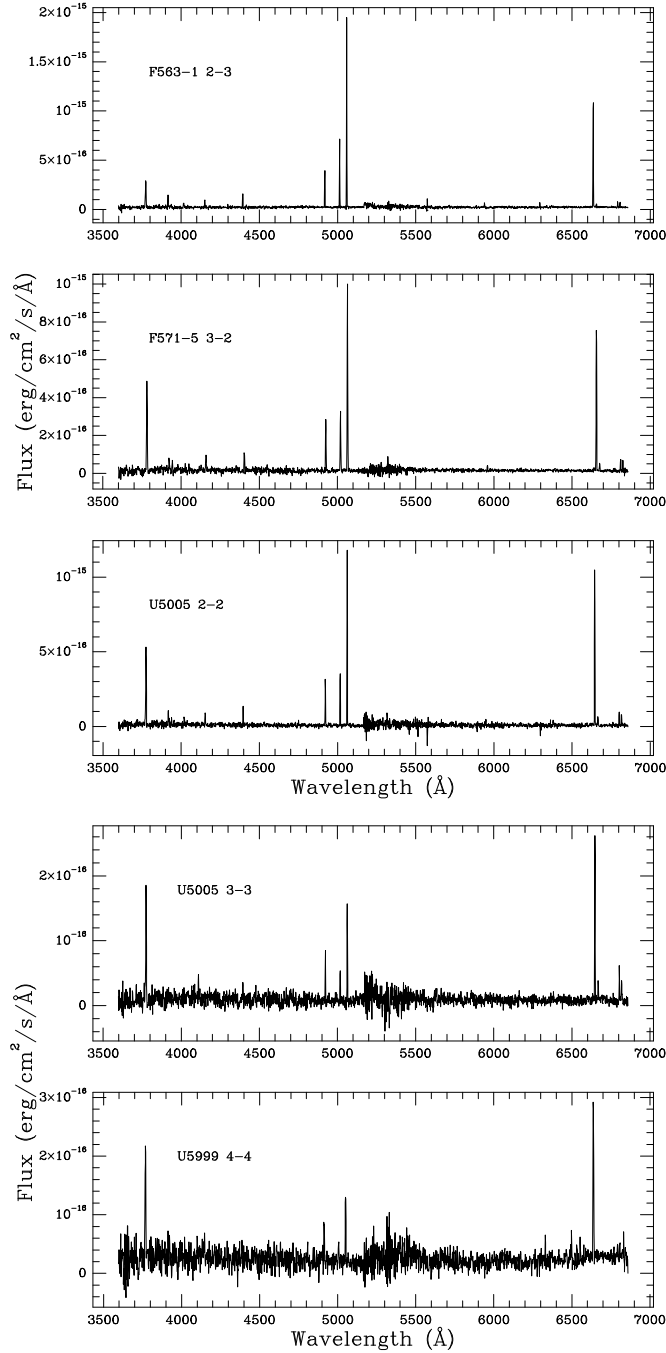


**Fig. 1.** Some examples of typical spectra of LSB galaxy HII regions.

We thus derive values of  $\log(\text{O}/\text{H}) = -3.81$  for F563-1 region 2-3, and  $\log(\text{O}/\text{H}) = -3.83$  for U5005 region 2-2. This should be compared with the empirical values derived for these regions (in the next section) of  $-3.99$  and  $-3.93$  respectively. The empirical values are consistent with the true values within 0.2 dex, which, as we will show in the next section, is the typical uncertainty of the empirical method.

#### 4.2. The strong line method

For spectra where the faint  $[\text{O III}]\lambda 4363$  line was not detected the empirical oxygen abundance indicating line ratio  $R_{23}$  was used. This ratio is defined as

$$R_{23} \equiv \frac{[\text{O II}]\lambda 3727 + [\text{O III}]\lambda\lambda 4959, 5007}{\text{H}\beta}.$$

Pagel et al. (1979) were the first to investigate the behaviour of this line ratio. The main problem with this empirical method is

**Table 4.** Oxygen: standard method

	F563-1:2-3	U5005:2-2
[O III] ratio	134.76	135.24
[SII] ratio	1.276	1.176
$T_e$ [O III] (K)	11525	11509
$T_e$ [O II] (K)	11068	11057
$n_e$ (cm <sup>-3</sup> )	165	291
log O <sup>++</sup> /H <sup>+</sup>	-3.92	-4.10
log O <sup>+</sup> /H <sup>+</sup>	-4.50	-4.17
log O/H	-3.81	-3.83
log (O/H) <sub>emp</sub>	-3.99	-3.93

the calibration: reliable measurements of the faint [O III] $\lambda$ 4363 line have to be available. For our purposes, we will use the calibration and models presented in McGaugh (1991).

For HII regions with low abundances  $R_{23}$  does not depend solely on oxygen abundance, but also on the degree of ionization of an HII region. This degree of ionization is given by the volume averaged nebular ionization parameter  $\langle U \rangle$ , which is defined by

$$U(R) = \frac{Q}{4\pi c N R^2}$$

where  $Q$  is the ionizing luminosity,  $N$  the gas density, and  $R$  the distance from the ionizing source.

$$\langle U \rangle = \frac{\int_0^{R_s} U(R) dV}{\int_0^{R_s} dV} = \frac{3Q}{4\pi c N R_s^2},$$

for constant density models, where  $R_s$  is the Strömgen radius.  $\langle U \rangle$  is then essentially the ratio of ionizing photon density to mass density.

In order to distinguish between the different degrees of ionization of the nebulae the ionization sensitive line ratio  $O_{32}$ , defined as

$$O_{32} \equiv \frac{[\text{O III}]\lambda\lambda 4959, 5007}{[\text{O II}]\lambda 3727}$$

is introduced.

This results in a model surface (Fig. 2) defined by contour lines with constant oxygen abundance and ionization parameter, as a function of  $R_{23}$  and  $O_{32}$ . The exact position of the grid in the  $R_{23}$ - $O_{32}$ -plane depends slightly on the assumed upper mass cut-off  $M_u$  of the IMF. The model presented here assumes  $M_u = 60M_\odot$ .

The oxygen abundance on the upper branch (drawn with solid lines) is relatively independent of the degree of ionization, while on the lower branch (dashed lines) the oxygen abundance cannot be determined reliably without taking  $O_{32}$  into account.

It is clear that most of this model surface is degenerate: once  $R_{23}$  and  $O_{32}$  are determined, there is still a choice between the low-abundance lower branch and the high-abundance upper branch. Especially for low  $R_{23}$  the difference between the two possibilities can be quite large.

The [N II] $\lambda$ 6583 line can be used to find out if a point lies on the upper or lower branch. The ratio [N II]/[O II] varies monotonically with abundance, and is not very sensitive to  $\langle U \rangle$

(see McCall et al. 1985). HII regions with  $\log([\text{N II}]/[\text{O II}]) > -1$  are on the upper branch. Most HSB spiral HII regions are found there (McCall et al. 1985). If  $\log([\text{N II}]/[\text{O II}]) < -1$  the HII regions are on the lower branch.

The model surface has a turnover region or fold at  $-3.9 < \log(\text{O}/\text{H}) < -3.4$ . In this region a large change of oxygen abundance corresponds to only a small interval in  $R_{23}$ . For HII regions occupying that part of the diagram an at least partly artificial crowding will occur around  $\log(\text{O}/\text{H}) = -3.6$ .

McGaugh (1991) showed that on the upper branch (solid lines;  $\log(\text{O}/\text{H}) > -3.4$  or  $Z > 0.5Z_\odot$ ) the uncertainty in the calibration of  $\log(\text{O}/\text{H})$  is  $\sim 0.1$  dex, and the uncertainty in the calibration of  $\langle U \rangle$  is  $\sim 0.15$  dex. On the lower branch (dashed lines;  $\log(\text{O}/\text{H}) < -3.9$  or  $Z < 0.15Z_\odot$ ) the calibration uncertainties are smaller, as the oxygen lines dominate the cooling process. The uncertainty in calibrating  $\log(\text{O}/\text{H})$  is  $\sim 0.05$  dex, and that in  $\langle U \rangle$  is  $\sim 0.1$  dex. To get an idea of the true uncertainties in the abundance determinations, these calibration uncertainties should thus be added to the observational uncertainties (see Sect. 5). For a more complete discussion of the calibration see McGaugh (1991).

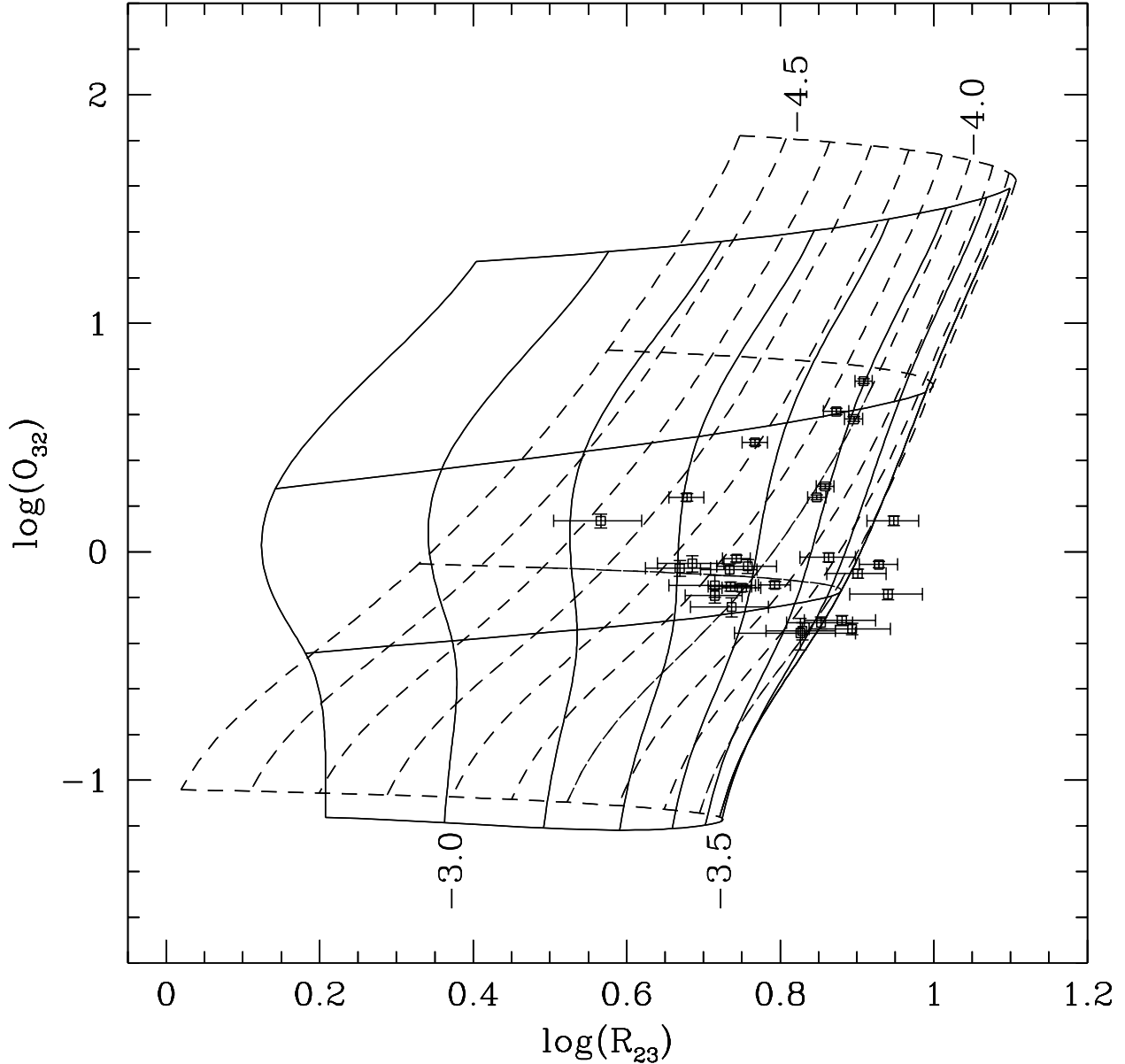
## 5. Oxygen Abundances

Figure 2 shows the reddening corrected positions of the measured HII regions in the diagram. In order to avoid spuriously large values of, especially,  $R_{23}$  we have omitted all HII regions where the peak value of the measured H $\beta$  line was less than  $3\sigma$  above the noise of the continuum. These regions are denoted in Table 2 by having their identification number (column 2) between brackets. The errorbars are determined by taking into account the uncertainties in the fluxes of the relevant lines using the continuum-offset procedure (see above). Note that the calibration uncertainties of the model (Sect. 4) are much larger than the formal errors in  $R_{23}$  and  $O_{32}$ .

All points are consistent with the model computed assuming an upper mass cut-off in the Initial Mass Function of  $M_u = 60M_\odot$  presented here. We therefore find no strong evidence for the existence of super-massive stars in the HII regions.

Figure 3 shows the reddening corrected [N II]/[O II] ratio as a function of  $R_{23}$  for our HII regions, along with those given in McCall (1985). We see that most of our HII regions have  $\log([\text{N II}]/[\text{O II}]) < -1$ , which implies that they are on the low-abundance lower branch of the model grid.

Oxygen abundances and ionization parameters are presented in Table 5, for those spectra where [N II]/[O II] could be determined. The errors were determined by projecting the continuum-offset uncertainties in  $R_{23}$  and  $O_{32}$  on the  $\log(\text{O}/\text{H})$  -  $\langle U \rangle$  -grid, and adding these in quadrature to the calibration uncertainties in  $\log(\text{O}/\text{H})$  and  $\langle U \rangle$  at these positions. In most cases the errors are dominated by the calibration uncertainties.



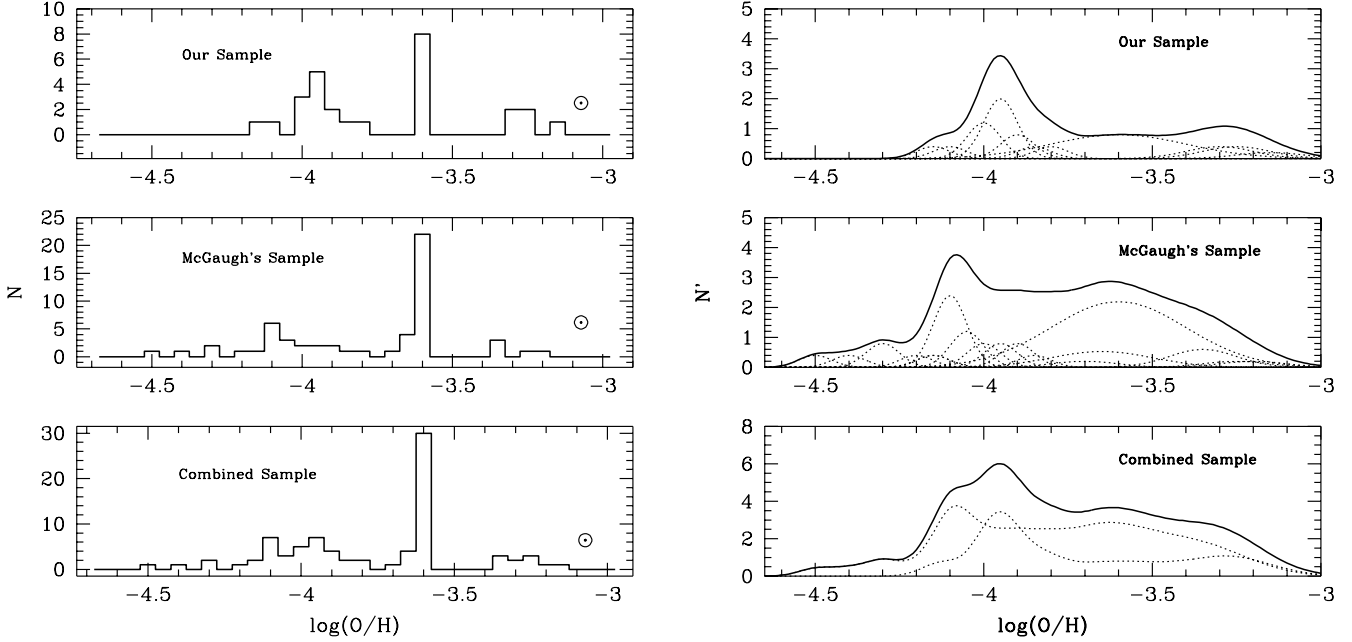
**Fig. 2.** Model grid of McGaugh (1991). The solid lines represent the upper branch; the dashed lines the lower branch. The vertical lines are lines of constant abundance; the horizontal lines of constant  $\langle U \rangle$ , with  $\log \langle U \rangle = -4$  at the bottom, and  $\log \langle U \rangle = -1$  at the top. The squares represent the values found for HII regions in our sample.

Table 6 presents the results for those spectra where  $[N \text{ II}]/[\text{O II}]$  was not measured, and the abundance determination was ambiguous. Both upper and lower-branch values are given.

Figure 4a shows histograms with the distribution of oxygen abundances. The top panel gives the distribution of abundances of HII regions from our sample, the middle panel shows the distribution of oxygen abundances of HII regions from the sample of McGaugh (1994) (his Table 3). The bottom panel shows the

distribution of both samples combined. Both samples have a few galaxies in common, but the number of HII regions that are in both samples is a few at most and any overlap will not influence the eventual results.

The peak in the histograms at  $\log(\text{O}/\text{H}) = -3.6$  in Fig. 4a is at least partly artificial. This is due to the fold at  $\log(\text{O}/\text{H}) = -3.6$  in the model grid of Fig. 2. We have attempted to correct for this in Fig. 4b. Here each of the histogram bins has been replaced by a gaussian with a width  $\sigma$  ( $= 0.43$  FWHM) equal to the uncertainty of the model grid at that abundance (e.g., the



**Fig. 4.** Left: Histograms of oxygen abundances of HII regions in LSB galaxies. Right: Histograms of oxygen abundances of HII regions in LSB galaxies. The histogram bars have been replaced by gaussians with error dependant widths. See text for more details.

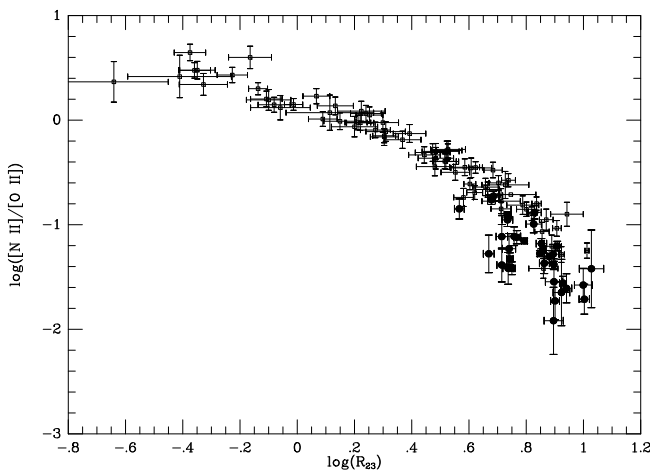


**Fig. 3.** Reddening corrected  $[NII]/[OII]$  ratios as function of  $R_{23}$  parameter. The filled circles represent our sample; the small squares the data of McCall et al (1985).

gaussian at  $\log(O/H) = -3.6$  has  $\sigma = 0.2$ ). The peak value was determined keeping the area under the gaussian equal to that of the corresponding histogram bar. As a result the peak at  $\log(O/H) = -3.6$  has been smeared out, and the distribution is almost flat, with maybe a slight peak at  $\log(O/H) \sim -4$ . This

peak might be the result of our selection method. Low abundance regions tend to be more ionized, and therefore brighter (e.g., Campbell 1988; Dopita & Evans 1986). Regardless of whether this effect is present or not, it is clear that within the abundance range shown by LSB galaxies, there is no preferred value.

With regard to the lowest abundances, Kunth & Sargent (1985) note that values of  $\log(O/H) = -4.3$  can already be reached after the first generation of massive stars. This might explain the cut-off in the abundance distribution around  $\log(O/H) = -4.3$  in Fig. 4. LSB galaxies are not primordial objects, but some of them appear to be very unevolved. Furthermore, to retain such low abundance values at the present epoch, these galaxies must have been quiescent over their entire life time, and some of them may not evolved significantly since their first epoch of star formation.

## 6. Reddening and extinction

The top panel in Fig. 5 contains a histogram of the reddenings towards the HII regions in our sample, corrected for the galactic contribution (Burstein & Heiles 1984). The middle panel contains a histogram for the sample of McGaugh (1994), while the bottom panel shows both samples combined. It is clear that the extinction in HII regions is low with  $\langle A_V \rangle = 3\langle E(B - V) \rangle \simeq$

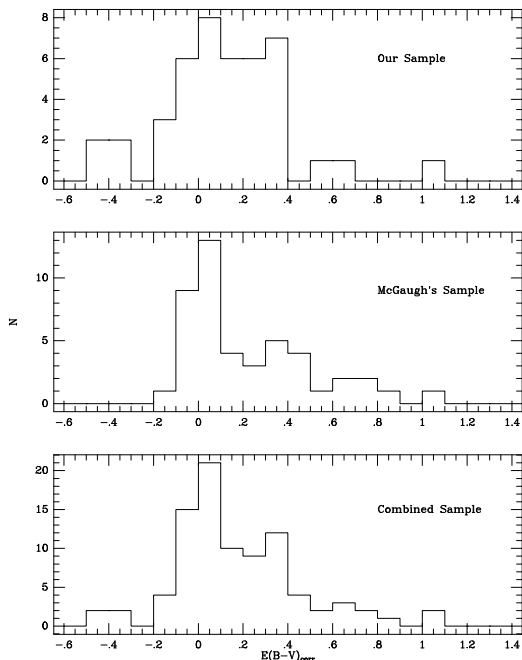


**Fig. 5.** Histograms of reddenings towards HII regions in LSB galaxies.

0.5 mag. For normal HSB galaxies extinction values are usually found to be up to a factor 6 larger (see e.g. Fig. 7 in Zaritsky et al. 1994). The conclusion that can be drawn from this, is that the reddening towards these HII regions is low, but at some sites some dust is present.

In the lowest abundance HII regions star formation is apparently able to proceed without much dust. These low reddenings also confirm that dust is not the cause of the low surface brightness of LSB galaxies.

## 7. Gradients

For galaxies F563-1, UGC 5005 and UGC 5999 we have enough measurements over a large enough radial range that we may attempt to investigate possible radial oxygen abundance gradients. We have plotted in Fig. 6 the abundances of the HII regions in these galaxies versus the deprojected radial distance, expressed in scale lengths. There is no clear trend of abundance with radius. Rather the oxygen abundance seems to be constant at  $-3.8 \pm 0.5$ .

To compare with other galaxies of similar Hubble type, we show in Fig. 6 the abundances of HII regions in 9 late-type Scd-Irr galaxies, taken from VCE (their Fig. 2). We have converted their half light radii  $R_d$  to disk scale lengths using the relation  $R_d = 1.678h$ , under the implicit assumption that the light distribution of their sample galaxies can be described by an exponential disk. As we are dealing with very late-type galaxies this assumption is most likely justified.

The VCE galaxies show a gradient of  $\sim 1$  dex over the range in radius sampled by the LSB galaxies. The LSB HII regions clearly do not follow this trend. The oxygen abundances

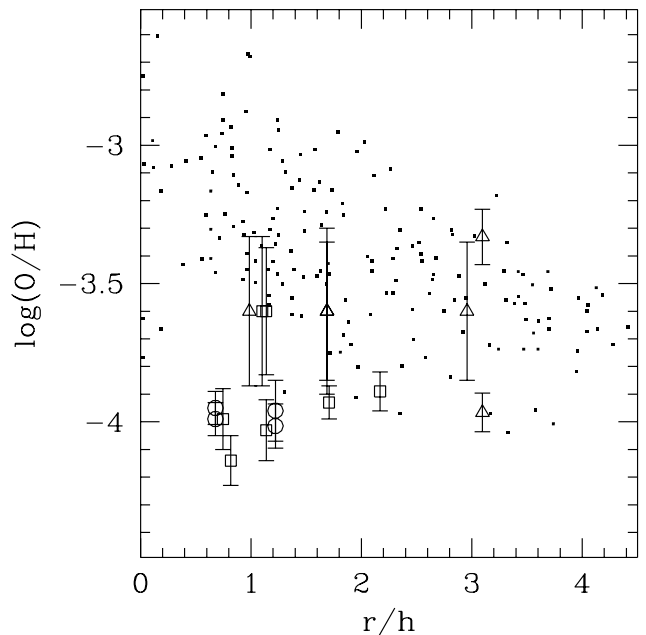


**Fig. 6.** Oxygen abundances in HII regions of 3 LSB galaxies. The true radial distance to the center (corrected for inclination effects) is expressed in optical scale lengths. The circles denote galaxy F563-1; the squares denote UGC 5005 and the triangles UGC 5999. No strong trend is seen. HSB late-type galaxies show a gradient of  $\sim 1$  dex in (O/H) over the radial range shown here.

in the LSB galaxies are lower at all radii, except in the very outer parts where the abundance values of the HSB and LSB galaxies appear to converge. The lack of abundance gradients in LSB galaxies may indicate that the picture of galaxies evolving from the inside out may not apply to LSB galaxies. It is usually assumed that the abundance and colour gradients found in galaxies indicate that the outer parts of galaxies are less evolved than the inner parts. The colours and abundances in LSB galaxies are comparable with those in the outer (most unevolved) parts of HSB galaxies. The absence of a radial abundance trend in the LSB galaxies suggests that these may have evolved at the same rate over their entire disk. Indeed, a spatially and temporally sporadic star formation rate, as is derived for LSB galaxies (e.g. Gerritsen & de Blok 1997), would not give rise to an abundance gradient.

Alternative explanations for the lack of a gradient may be the infall of metal-poor gas from high above the planes of these galaxies. However, because of the low star formation activity in LSB galaxies it is not likely that large amounts of gas can have been blown out in the past. If gas infall is a major factor, this must be “primordial” gas, left over from when the LSB galaxies were formed.

A second alternative is that the disks of LSB galaxies are still settling in their final configuration. Gas from larger radii is slowly diffusing inward, causing density enhancements where conditions for star formation may be favourable. This is qual-

itatively consistent with the finding that most of the star forming regions in LSB galaxies are found towards the outer radii of the stellar disk. If star formation in LSB galaxies needs to be stimulated by external conditions (like infall), and is not self-propagating, this building up of the disk would not give rise to an abundance gradient. If every radius would go through one cycle of star formation before fading, after which star formation would move on to larger radii, this would cause a colour gradient (as is observed) but no abundance gradient. Note that though this evolution “from the inside out” is different from the standard picture mentioned above. In that picture each radius continues evolving, with the inner radii going through more star formation cycles than the other radii. Clearly, the scenario described here is only a crude ad-hoc attempt to explain the lack of gradient. It would have to be tested by modelling, and supported by more abundance data.

In this respect the discussion presented in Edmunds & Roy (1993) is of interest. They show that steep abundance gradients in gas-rich disk galaxies seem to require the presence of unbarred spiral structure. The abundance gradients disappear at the same absolute magnitude that spiral structure ceases ( $M_B \sim -17$ ) and are considerably shallower in galaxies with a strong bar.

The late-type LSB galaxies in general show only a faint spiral structure, and have  $M_B \sim -17.5$ . Their feeble spiral structure may thus be related with the lack of abundance gradients. Edmunds & Roy (1993) offer two possible explanations. The variation with radius of the frequency with which interstellar material passes through a spiral pattern may result in a declining star formation rate with radius. This would set up an abundance gradient. At lower absolute magnitudes star formation will still continue, but the spiral pattern would be absent. This would result in a star formation rate which is much more uniform across the disk than in strong spirals. Alternatively, if non-circular motions are relatively more important the resulting mixing may also homogenize the chemical composition of the interstellar medium.

Although we realize that it is easy to over-interpret data of such a limited dynamic range, we conclude that the lack of abundance gradients confirms the evolutionary picture of quietly evolving LSB galaxies with only local processes regulating their evolution.

## 8. Conclusions

The oxygen abundances in 64 HII regions in 12 LSB galaxies have been measured. Oxygen abundances are low. No region with solar abundance has been found, and most have oxygen abundances that are  $\sim 0.5$  to 0.1 solar. No strong radial oxygen abundance gradients are found. The abundance seems to be constant, rather, as a function of radius, supporting the picture of quiescently and sporadically evolving LSB galaxies.

*Acknowledgements.* We thank the referee Dr. Smartt for his constructive comments which have helped improve the presentation of these data.

The William Herschel Telescope is operated on the island of La Palma by the Isaac Newton Group in the Spanish Observatorio del Roque de los Muchachos of the Instituto de Astrofísica de Canarias.

## References

- Bothun G.D., Impey C.D., McGaugh S.S. 1997, PASP in press  
 Burstein D., Heiles C. 1984, ApJS 54, 33  
 Campbell A. 1988, ApJ 335, 644  
 Campbell A., Terlevich R., Melnick J. 1986, MNRAS 223, 811  
 de Blok W.J.G., van der Hulst J.M., Bothun G.D. 1995, MNRAS 274, 235  
 De Robertis M.M., Dufour R.J., Hunt R.W. 1987 JRASC 81, 195  
 Dopita M.A., Evans I.N. 1986, ApJ 307, 431  
 Edmunds M.G., Roy J.-R. 1993, MNRAS 261, L17  
 Gerritsen J.P.E., de Blok W.J.G. 1998, A&A submitted  
 Henry R.B.C., Howard J.W. 1995, ApJ 438, 170  
 Kennicutt R.C., Garnett, D.R. 1996, ApJ 456, 504  
 Kunth D., Sargent W.L.W. 1986, ApJ 300, 496  
 McCall L.M., Rybski P.M., Shields G.A. 1985, ApJS 57, 1  
 McGaugh S.S. 1991, ApJ 380, 140  
 McGaugh S.S. 1994, ApJ 426, 135  
 Mo H. J., McGaugh S.S., Bothun G. D. 1994, MNRAS 267, 129  
 Osterbrock D.E. 1989, Astrophysics of Gaseous Nebulae and Active Galactic Nuclei, Mill Valley: University Science Books  
 Pagel B.E.J., Edmunds M.G., Blackwell D.E., Chun M.S., Smith G. 1979, MNRAS 193, 219  
 Savage B.D., Mathis J.S. 1979, ARA&A 17, 73  
 Smartt S.J., Rolleston W.R.J. 1997, A[J 481, L47  
 van der Hulst J.M., Skillman E.D., Smith T.R., Bothun G.D., McGaugh S.S., de Blok W.J.G. 1993, AJ 106, 548  
 Vila-Costas M.B., Edmunds M.G. 1992, MNRAS 259, 121  
 Zaritsky D., Kennicutt R.C., Huchra J.P. 1994, ApJ 420, 87

**Table 2.** Line ratios

Galaxy	HII	[O II] $\lambda 3727$	H $\gamma$ $\lambda 4861$	[O III] $\lambda 4959$	[O III] $\lambda 5007$	H $\alpha$ $\lambda 6563$	[N II] $\lambda 6583$	[S II] $\lambda 6717$	[S II] $\lambda 6731$
F561-1	1-1	2.566		0.447	1.836	2.994	0.524	0.595	0.350
	1-2	2.862		0.725	1.948	3.224	0.169	0.421	0.249
F563-1	2-1	3.158	0.552	0.556	1.472	2.040	0.130	0.328	0.209
	(2-2)	3.383		0.425	1.688	1.931	0.199	0.489	0.277
	*2-3	1.232	0.417	1.755	5.118	3.079	0.088	0.171	0.134
	(2-4)	4.733		0.652	2.501	5.234	0.417	0.926	0.543
	4-1	3.465		0.451	1.538	3.805	0.226	0.673	0.331
	4-2	1.636	0.270	1.586	4.646	3.758	0.114	0.294	0.202
F563-V1	(4-3)	5.003		0.592	2.270	9.007	0.513	2.334	1.240
	3-2	3.745		1.418	3.704	2.690		0.362	0.246
F563-V2	(3-3)	3.522		0.826	2.647	2.855		0.596	0.541
	2-1	1.748	0.316	0.916	2.105	2.465	0.302	0.293	0.268
	2-2	1.460	0.328	1.181	3.211	3.366	0.150	0.347	0.273
	2-3	3.754	0.468	0.887	2.660	3.620	0.249	0.466	0.321
	4-1	4.515		0.942	3.027	4.450	0.285	0.973	0.897
	4-2	5.058		0.754	1.779	4.163	0.505	0.909	1.296
F568-3	2-1	2.955	0.563	0.726	1.743	3.540	0.489	0.456	
F568-V1	(3-1)	6.641		1.761	1.582	4.391	0.392	0.898	1.234
F571-5	*3-1	1.460	0.275	1.539	4.467	2.408	0.827::	0.140	0.339
	*3-2	2.460	0.404	1.194	3.566	2.770	0.144	0.225	0.224
F571-V1	(3-1)	2.967		0.639	2.133	3.919			
U1230	1-1	1.557		0.662	1.464	3.041	0.247	0.270	0.294
	3-1			0.871	2.050	3.283	0.282		
	(3-2)			1.511	2.343	1.975		0.308	0.419
U5005	(3-6)			0.718	2.531	4.955	0.568	1.619	1.010
	2-1	2.621		0.361	0.964	3.192		0.302	0.450
	*2-2	2.577	0.424	1.130	3.333	3.535	0.206	0.294	0.250
	(2-3)	3.165	0.927	1.095	3.404	2.583			
	2-4	4.652		0.653	1.441	4.074	0.803	0.688	0.523
	2-5			0.389	1.662	3.168	0.571	0.503	0.683
	(2-6)	4.483		0.830	3.066	3.519	0.148	0.488	0.513
	(2-7)	4.363		2.251	4.053	3.127	0.195		
	3-2	2.526		0.594	1.548	1.803	0.133	0.397	0.357
	3-3	3.073	0.471	0.603	2.050	3.374	0.324	0.620	0.432
U5999	3-5	3.032		0.388	1.768	2.854	0.233	0.553	0.328
	4-1	3.618		0.717	1.874	4.169	0.511	0.525	0.405
	(4-2)	5.167		1.140	3.761	6.087	0.411	1.103	0.618
	3-1	5.281		0.887	2.554	3.770	0.218	0.702	0.379
	3-2	4.788		0.566	1.779	4.333	0.686	1.105	0.671
	3-3	4.418		0.859	2.684	3.305	0.108	0.571	0.479
U5999	3-4	3.316		0.504	1.804	3.227	0.159	0.383	0.212
	4-1	5.365		1.144	1.322	2.723	0.280	0.497	0.872
	4-4	3.190		0.511	1.736	4.224	0.822	0.311	0.291
Galaxy	HII	[O III] $\lambda 4363$	H $\delta$ $\lambda 4101$	He $\lambda 3970$	H $\eta$ $\lambda 3889$	[Ne III] $\lambda 3869$	He I $\lambda 5876$		
F563-1	2-3	0.051	0.191	0.189	0.092	0.371	0.132		
F571-5	3-1					0.382	0.134		
	3-2		0.317	0.118	0.171	0.206	0.091		
U5005	2-2	0.033	0.291	0.204	0.144	0.343	0.129		

Note: HII regions with their identification number between brackets are not used for further analysis (see Sect. 5).

**Table 3.** Miscellaneous Fluxes

Galaxy	HII	$W_\lambda$ ( $H\alpha$ )	[O II] $\lambda 3727$	[O III] $\lambda 4959$	H $\alpha$ $\lambda 6563$	[N II] $\lambda 6583$	[S II] $\lambda 6717$	[S II] $\lambda 6731$	H $\beta$
F563-V1	3-1	16		88	76				<29
F568-3	2-2	24			78	21			<15
	2-3	7			115	33	39		<45
	2-4	29			316	69	85		<40
F568-V1	3-2	11	467		377	115	122	145	<58
	3-3	24	371	342	275			68	<54
	3-4	157	328		188	21			<45
U1230	1-2	91	30		317	29	32	39	<68
	1-3	89			304	32	46	33	<61
	3-5	86			72	55	109		<57
U5005	3-1	40			174	20	52	40	<28
	3-4	33	306	178	341	42	94	62	<49
U5999	4-2	50	568		621	60	220	96	<71
	4-3	44	29		529	26	40	61	<12
U6614	1-1	18			213	118			<60
	1-2	34			243	76			<60
	2-1	39			251	97	32		<22
	2-2	349			57				<14
	4-a	17	776		1294	552			<124
	4-1	27			1307	576			<160
	4-2	10			187	122			<106

**Table 5.** Oxygen Abundances

Galaxy	HII	log O/H	$\sigma_{O/H}$	log $\langle U \rangle$	$\sigma_{\langle U \rangle}$
F561-1	1-1	-3.28	0.12	-2.69	0.16
	1-2	-4.03	0.06	-2.89	0.10
F563-1	2-1	-4.01	0.08	-3.06	0.11
	2-3	-3.99	0.06	-2.05	0.10
	4-1	-3.96	0.11	-3.10	0.11
	4-2	-3.95	0.06	-2.22	0.10
F563-V2	2-1	-3.25	0.10	-2.34	0.15
	2-2	-4.17	0.06	-2.36	0.10
	2-3	-3.80	0.23	-2.85	0.20
	4-1	-3.60	0.24	-2.86	0.20
	4-2	-3.60	0.28	-3.12	0.20
F568-3	2-1	-3.32	0.11	-2.74	0.15
F571-5	3-2	-3.93	0.06	-2.53	0.10
U1230	1-1	-3.16	0.11	-2.43	0.15
U5005	2-2	-3.93	0.06	-2.58	0.10
	2-4	-3.60	0.23	-3.08	0.20
	2-5	-3.60	0.27	-3.09	0.23
	3-2	-4.14	0.09	-2.95	0.11
	3-3	-3.99	0.11	-2.92	0.11
	3-5	-4.03	0.11	-3.01	0.11
	4-1	-3.89	0.07	-2.99	0.10
U5999	3-1	-3.60	0.25	-2.99	0.20
	3-2	-3.60	0.27	-3.14	0.20
	3-3	-3.60	0.25	-2.91	0.20
	3-4	-3.97	0.07	-3.01	0.10
	4-1	-3.60	0.30	-3.16	0.20
	4-4	-3.33	0.10	-2.83	0.15

**Table 6.** Ambiguous Abundances

Galaxy	HII	log O/H	$\sigma_{O/H}$	log $\langle U \rangle$	$\sigma_{\langle U \rangle}$	log O/H	$\sigma_{O/H}$	log $\langle U \rangle$	$\sigma_{\langle U \rangle}$
F563-V1	3-2	-3.30	0.16	-2.57	0.15	-3.60	0.23	-2.66	0.20
F571-5	3-1	-3.39	0.11	-1.98	0.15	-4.02	0.05	-2.20	0.10